



Published in final edited form as:

ACS Nano. 2010 February 23; 4(2): 1049–1059. doi:10.1021/nn901213a.

## Host-guest Interaction Mediated Polymeric Assemblies: Multifunctional Nanoparticles for Drug and Gene Delivery

Jianxiang Zhang<sup>1</sup>, Hongli Sun<sup>1</sup>, and Peter X Ma<sup>1,2,3,\*</sup>

<sup>1</sup> Department of Biologic and Materials Sciences, University of Michigan, Ann Arbor, MI 48109, USA

<sup>2</sup> Macromolecular Science and Engineering Center, University of Michigan, Ann Arbor, MI 48109, USA

<sup>3</sup> Department of Biomedical Engineering, University of Michigan, Ann Arbor, MI 48109, USA

### Abstract

Novel core-shell structured nano-assemblies are assembled by a  $\beta$ -cyclodextrin containing positively charged host polymer and a hydrophobic guest polymer. The hydrophobic core of this type of assemblies serves as a nano-container to load and release the hydrophobic drugs, while the positively charged hydrophilic shell is able to condense the plasmid DNA and achieve its transfection/expression in osteoblast cells. These assemblies may be used as a new generation of multi-functional nano-carriers for simultaneous drug delivery and gene therapy.

### Keywords

host-guest interactions; polymer assemblies; multifunctional nanoparticles; drug delivery; gene delivery

---

Multi-functionalized nanocarriers are attractive in pharmaceuticals, medical imaging, biomedical engineering, and gene therapy.<sup>1</sup> For instance, drug delivery, cell targeting and/or multi-modal imaging can be simultaneously achieved by multifunctional inorganic nanoparticles or nanocrystals, inorganic-organic hybrid nanoparticles and polymeric assemblies.<sup>2-9</sup> Studies based on these versatile pharmaceutical nanocarriers have provided profound insights on the intracellular or *in vivo* distribution, and valuable information on the spatial and temporal interactions of delivery carriers with cells and tissues as well as their intracellular interactions. In addition, multi-functional nanoparticles have also been employed to implement the simultaneous gene delivery, drug delivery and imaging.<sup>6, 10-14</sup> Using cyanine dye (Cy5.5) labeled magnetic nanoparticles conjugated to a synthetic small interfering RNA (siRNA) duplex, Moore and coworkers were able to achieve the *in vivo* transfer of siRNA and the simultaneous imaging of its accumulation in tumors by high-resolution magnetic resonance imaging and near-infrared *in vivo* optical imaging.<sup>15</sup> Proton-sponge coated quantum dots were employed by Nie and Gao *et al.* for siRNA delivery and intracellular imaging.<sup>16</sup>

While these nanocarriers allow the real-time tracking and ultrastructural localization of siRNA delivery system, combining drug delivery and gene therapy in one particle has the potential to

---

\*To whom correspondence should be addressed: Prof. Peter X Ma, Department of Biologic and Materials Sciences, Macromolecular Science and Engineering Center, Department of Biomedical Engineering, University of Michigan, Ann Arbor, MI 48109, USA; mapx@umich.edu.

Supporting Information Available. <sup>1</sup>H NMR, FT-IR and fluorescence spectra, and titration curves. This material is available free of charge via the Internet at <http://pubs.acs.org>.

enhance the transfection efficiency or to achieve a synergistic/combined effect of drug and gene therapies.<sup>17-20</sup> By co-delivering inflammatory suppressors and plasmid DNA (pDNA) through liposomes, Huang and coworkers developed a non-immunostimulatory gene vector (safeplex), which can inhibit the inflammatory toxicity induced by cationic lipids and CpG motif of pDNA.<sup>21</sup> Using cationic core-shell nanoparticles self-assembled from an amphiphilic copolymer, co-delivery of paclitaxel and pDNA/siRNA was achieved by Yang et al.<sup>22</sup> Both *in vitro* and *in vivo* studies demonstrated that these nanoparticles could suppress cancer growth more efficiently compared with delivery system containing either drug or therapeutic gene alone. Recently, polymeric micelles based on polyethyleneimine grafted poly( $\epsilon$ -caprolactone) have also been employed as the dual carriers of an anticancer drug and gene to achieve the synergistic effects.<sup>23</sup> Although only a few studies regarding multifunctional pharmaceutical nanocarriers based on polymers have been reported this far, such delivery systems already showed great potentials to function as highly efficient and specialized carriers for drugs, genes, and diagnostic agents.

On the other hand, due to its excellent biocompatibility,  $\beta$ -cyclodextrin ( $\beta$ -CD) has been widely used as a host unit to construct delivery carriers.<sup>24</sup> Camptothecin conjugated  $\beta$ -cyclodextrin-based polymers have been synthesized to assemble into nanoparticles for tumor therapy by Davis's group.<sup>25, 26</sup> In addition,  $\beta$ -CD containing polycations were developed for siRNA delivery.<sup>27, 28</sup> Most importantly, both delivery systems have been successfully developed to clinical trials. The aim of this contribution is to develop novel multifunctional polymeric nano-assemblies for simultaneous drug and gene delivery. The core-shell structured nanocarriers developed herein are assembled through a host-guest interaction by a  $\beta$ -cyclodextrin containing cationic polymer and a hydrophobic polymer. The hydrophobic core serves as a nanocontainer for lipophilic drugs, while the cationic shell can condense pDNA. Functioning as multifunctional nano-vehicles, these polymeric assemblies can simultaneously deliver both hydrophobic drugs and genes.

## Results and Discussion

As a proof of concept, we selected a branched polyethyleneimine (PEI) as a scaffold polymer, onto which  $\beta$ -CDs were conjugated as the host units that can complex with a guest hydrophobic polymer to mediate the assembly process. By a nucleophilic substitution reaction between 6-mono-tosyl  $\beta$ -CD and amino group of PEI,  $\beta$ -CD conjugated PEI (PEI-CD) was synthesized. Figure S1b shows <sup>1</sup>H NMR spectrum of PEI-CD. In addition to the chemical shift at 2.5-3.0 ppm, the appearance of signals at 3.4-4.0 and 5.1 ppm, which are characteristic signals of protons from  $\beta$ -CD, suggested the successful conjugation of  $\beta$ -CD units. Moreover, as shown in Figures S2a and b of FT-IR spectra of PEI and PEI-CD, absorption at 1033 cm<sup>-1</sup> due to –C–O– groups increased significantly compared with that of PEI, which also verified the introduction of  $\beta$ -CD units onto PEI scaffold. Calculation based on <sup>1</sup>H NMR spectrum indicated that about 13  $\beta$ -CD groups were conjugated onto each PEI chain. On the other hand, poly( $\beta$ -benzyl L-aspartate) (PBLA), a hydrophobic polymer with flanking benzyl groups was selected as a model guest polymer. The molecular weight of PBLA synthesized by a ring-opening polymerization was about 2000 as determined by a matrix-assisted laser desorption/ionization time-of-flight (MALDI-TOF) mass spectrometer.

By a modified dialysis procedure, assemblies based on PEI-CD/PBLA were prepared. A preliminary FT-IR measurement was performed to confirm the incorporation of PBLA component into the assemblies. As shown in Figure S2c, in addition to absorptions due to PEI-CD, new peaks corresponding to PBLA appeared, especially that at 1735 cm<sup>-1</sup>, which is a characteristic stretching vibration of carbonyl in PBLA. Accordingly, this result indicated the presence of PBLA component in the obtained assemblies. Unless stated otherwise, all the following studies were based on the assemblies prepared by the formulation with a weight ratio

(PEI-CD to PBLA) of 10:3. The morphology of assemblies was characterized using transmission electron microscopy (TEM), atomic force microscopy (AFM) and scanning electron microscopy (SEM). As shown in Figure 1a of TEM image, spherical assemblies can be observed. Statistical analysis based on TEM images suggested that the average size was 95 nm. The spherical morphology of assemblies was further demonstrated by AFM and SEM images, which are illustrated in Figures 1c and d. The number-averaged size determined by dynamic light scattering (DLS) was 90.6 nm (Figure 2), and this result was consistent with TEM and SEM observation. The combination of TEM, AFM and SEM results pointed to the conclusion that spherical nanoparticles can be assembled by PEI-CD in the presence of PBLA. Thus obtained nano-assemblies were stable enough to be characterized by AFM and SEM. In addition, by staining with phosphotungstic acid (PTA), we were able to directly observe the core-shell structure of PEI-CD/PBLA assemblies. As shown in Figure 3, a dark shell can be clearly observed. Since PTA preferentially stains hydrophilic micro-domains, this dark shell should correspond to hydrophilic segments of PEI chains.

Fluorescence measurement was then employed to provide information on the core of assemblies, and pyrene was used as a probe. Figure 4a shows the normalized emission spectra of pyrene in the presence of PEI-CD/PBLA derived assemblies. The fluorescence band from 370 to 420 nm is the characteristic emission of excited pyrene monomer, while the broad band extending from 420 to 600 nm is ascribed to the pyrene excimer. With the increase in assemblies' concentration, a significant enhancement in excimer intensity can be observed. Plots of concentration dependent changes in intensity ratios of  $I_{338}/I_{333}$ ,  $I_3/I_1$  and  $I_E/I_M$  are shown in Figure 4b. Significant increase in the values of  $I_{338}/I_{333}$ ,  $I_3/I_1$  and  $I_E/I_M$  can be observed for pyrene as the concentration of PEI-CD/PBLA assemblies increased to a certain point. Based on  $I_3/I_1$  data, a critical concentration of 0.04 mg/mL was obtained. No significant changes in  $I_E/I_M$ , however, were found in the case of  $\beta$ -CD (Figure S3). Furthermore, the values of  $I_3/I_1$  for PEI-CD/PBLA assemblies are comparable with those of polymeric micelles based on polyethylene glycol-block-poly( $\beta$ -benzyl L-aspartate) (PEG-*b*-PBLA), which were significantly larger than those for  $\beta$ -CD. These observations indicated that assemblies based on PEI-CD/PBLA possessed a core similar to that of PEG-*b*-PBLA micelles. In other words, the core of PEI-CD/PBLA assemblies might be mainly composed of hydrophobic PBLA.

Further information on the microviscosity of inner core of assemblies was provided by  $^1\text{H}$  NMR and fluorescence anisotropy. As shown in Figure S1c, no proton signals corresponding to PBLA can be observed for assemblies based on PEI-CD/PBLA in  $\text{D}_2\text{O}$ . However, signals at 7.3 and 5.0 ppm that are characteristic peaks of protons related to benzyl group, are evident in  $\text{DMSO-}d_6$ . This indicates that the cores of these assemblies are mainly comprised of PBLA chains with limited mobility, and therefore this type of assemblies possesses a rigid core. In the case of fluorescence depolarization study, 1, 6-diphenyl-1, 3, 5-hexatriene (DPH) was used as a fluorophore. The magnitude of  $r$  measured for DPH in an aqueous solution of PEI-CD/PBLA based assemblies was about 0.26, which was even larger than that for PEG-*b*-PBLA based micelles ( $r=0.23$  in this case). This result again suggested that the cores of assemblies based on PEI-CD/PBLA are essentially rigid.

As a summary, above results suggested that core-shell structured nano-assemblies could be formed by PEI-CD in the presence of PBLA. PBLA-rich micro-domain formed the hydrophobic core, while positively charged PEI segments served as the hydrophilic shell. Since there is an inclusion interaction between benzyl group and CD unit, which has been well documented,<sup>29</sup> this host-guest supramolecular interaction should contribute to the assembly of PEI-CD/PBLA. The assembly process is schematically illustrated in Scheme 1. With the introduction of PBLA into the aqueous solution of PEI-CD, the complexation interaction between benzyl group and CD leads to the formation of pseudo-amphiphilic polymers which are able to assemble into nanoparticles. Additional PBLA chains can also be incorporated

considering the existence of hydrophobic interaction. In addition, as no peaks corresponding to PEI-CD chains can be observed from DLS curve, almost all the PEI-CD macromolecules might participate in the assembly process.

For assemblies to be used as drug/gene delivery carriers, the stability and dispersion behavior after the reconstitution from a freeze-dried formulation are important issues.<sup>30</sup> Frequently, the freeze-drying process may result in the formation of large aggregates, which in turn influences the therapeutic efficacy. As preliminary stability studies, the effect of freeze-drying/reconstitution on the size and morphology of assemblies was evaluated. Figure 1b shows the TEM image of PEI-CD/PBLA based assemblies after freeze-drying and reconstitution. Spherical assemblies still can be observed when the freeze-dried samples were reconstituted in an aqueous medium. In addition, size distribution of assemblies shown in Figure 2 revealed that the freeze-drying and subsequent reconstitution had no significant effect on the particle size. The mean size of assemblies after freeze-drying/reconstitution was 92.3 nm, which was essentially identical to that before freeze-drying (90.6 nm). This result indicates that this type of assemblies exhibit a good dispersion behavior after freeze-drying.

In order to address the capability of drug loading and release using PEI-CD/PBLA assemblies, dexamethasone (DMS), a highly hydrophobic steroidal anti-inflammatory drug, was selected. By a similar dialysis procedure, DMS-containing assemblies were prepared. According to UV measurement, 5.8% DMS was loaded. The TEM image shown in Figure 1e suggested that the incorporation of DMS almost had no effect on the morphology of assemblies. Similar to the blank samples, a freeze-drying/reconstitution cycle had no significant impact on both particle size and size distribution of DMS containing assemblies (Figure 2). The number-average size before freeze-drying and after reconstitution was 74 and 78 nm, respectively. Figure 5 shows the cumulative release profile of DMS. A two stage release behavior was observed: a rapid release within the first two days followed by a sustained release phase. It was also found that the release of DMS from PEI-CD/PBLA assemblies can be sustained for about one month. This result suggests that the core of PEI-CD/PBLA assemblies offer a nano-container to load and deliver hydrophobic drug.

A titration experiment was performed to determine the pKa values of both PEI-CD and PEI-CD/PBLA based on pH dependent protonation curves. As shown in Figure S4, a similar two-stage protonation curve was observed for both PEI-CD and PEI-CD/PBLA. From which the pKa values of the primary and secondary amino groups were determined to be 10.5 and 6.5, respectively. This result suggests that the presence of PBLA did not significantly affect the protonation behavior of PEI-CD. In addition, zeta potential measurement revealed that the  $\zeta$ -potential was 38.3 mV for PEI-CD/PBLA assemblies, indicating the positively charged surface of these nanoparticles. These results also support the core-shell structure of PEI-CD/PBLA assemblies as mentioned above.

As well known, polyplexes, i.e. the nanoparticles formed by electrostatic complexation of cationic polymers and DNA, have been widely employed as non-viral transfection vectors. Herein, polyplex-like nano-vehicles were prepared by directly mixing pDNA with PEI-CD/PBLA assemblies at various weight ratios. Polyplex solutions thus obtained remained stable over a long-time storage, and no precipitate was observed over the entire range of weight ratios examined. To demonstrate the condensation capability of PEI-CD/PBLA nano-assemblies to pDNA, a gel retardation assay was performed. As shown in Figure 6a, the amount of migrating free pDNA gradually decreased with an increase in the weight ratio, indicating the complex formation between pDNA and PEI-CD/PBLA assemblies. Complete retardation of pDNA was achieved when the weight ratio increased to above 0.6. This was further confirmed by ethidium bromide (EtBr) exclusion assay. Whereas EtBr fluorescence intensity would be greatly enhanced by forming an intercalating complex with double helical polynucleotides,<sup>31</sup> the complexation

between DNA and a cationic polymer would result in a quenching of EtBr fluorescence. This characteristic of EtBr is frequently utilized to estimate the degree of pDNA condensation through complexation with a cationic polymer or positively charged nanoparticles.<sup>32</sup> As shown in Figure 6b, the fluorescence intensity of EtBr decreased with an increase in the weight ratio, which leveled off when the weight ratio was above 0.7. This decreased fluorescence is consistent with the gradual complexation of PEI-CD/PBLA assemblies with pDNA, inhibiting the intercalation of EtBr into pDNA as a result of coil-to-globule transition of pDNA.<sup>33</sup> Note that the apparent end point of the coil-to-globule transition, evaluated based on EtBr exclusion, was consistent with the result of the gel retardation assay shown in Figure 6a.

According to the above results of gel retardation as well as EtBr exclusion assays, pDNA could be essentially complexed with PEI-CD/PBLA assemblies to form a condensed structure when the weight ratio was higher than 0.6. To gain insight into the physicochemical properties of these complexes, DLS and  $\zeta$ -potential measurements were then performed. As can be seen from Figure 7, the introduction of pDNA resulted in an increase in particle size (compare with Figure 2). However, increase in the weight ratio of PEI-CD/PBLA to pDNA led to a decrease in particle size. When the weight ratio increased from 2 to 20, the mean size decreased from 150 to 116 nm. As suggested by previous studies, this phenomena was attributed to the formation of nonstoichiometric complexes.<sup>33, 34</sup>  $\zeta$ -Potential was significantly increased with the increase in the weight ratio of PEI-CD/PBLA to pDNA. For formulation with a weight ratio of 20:1,  $\zeta$ -potential was about 37, which was close to that of blank PEI-CD/PBLA assemblies. A similar phenomenon was observed previously for polyion complex (PIC) micelles based on oppositely charged polyelectrolytes.<sup>33, 35</sup>

*In vitro* transfection experiment was performed with MC3T3-E1 osteoblast cells using the polyplexes prepared at various weight ratios. Although both the retardation and EtBr exclusion assay suggested that a complete condensation of pDNA was achieved when the weight ratio was above 0.6, effective transfection was not observed for formulations with a weight ratio slightly higher than 0.6. An appreciable increase in the transfection efficiency in the region of weight ratio  $\geq 4$  was observed as shown in Figure 8a. This trend of increased gene transfection with the weight ratio was correlated with the increase in  $\zeta$ -potential of polyplexes as shown in Figure 7. Nevertheless, further increase in weight ratio may lead to a decrease in transfection. Luciferase activity reached a maximum at a weight ratio of 10. In this case, intense red fluorescence can be observed for the cultured cells transfected with polyplexes based on PEI-CD/PBLA assemblies, while almost no transfected cells were found for the control group (Figure 8b), indicating the former to have transfected a significant number of cells and resulted subsequent gene expression. However, it should be noted that the transfection efficiency of our polyplexes was lower than that based on PEI alone at this moment. Further optimizing the delivery system by tailoring PEI-CD structure as well as modulating the assemblies' composition is necessary to increase the transfection activity while keep the lower cytotoxicity at the same time. Polyplexes based on DMS containing assemblies (the weight ratio of assemblies to pDNA was 10:10) were also prepared for transfection. Physicochemical characterization indicated that the loading of DMS had no influence on the resultant polyplexes compared with those based on the blank assemblies of the same formulation. A slight increase in transfection efficiency was observed for DMS containing polyplexes compared to the counterpart without DMS. This enhancement should be related to the DMS induced dilation of nuclear pore complexes.<sup>36</sup> The increased nuclear translocation of macromolecules and nanoparticles by DMS has also been confirmed by other researchers.<sup>37, 38</sup>

The low cytotoxicity of vectors is a crucial aspect for successful nonviral gene delivery. In this study, the cytotoxicity of polyplexes was evaluated by cell proliferation assay under the same conditions used for gene transfection. As shown in Figure 9, in comparison with PEI-CD, PEI-CD/PBLA assemblies showed low cytotoxicity. Interestingly, the cytotoxicity was drastically

lowered for assemblies loaded with DMS. As an anti-inflammatory and immunosuppressive drug, DMS can inhibit proinflammatory cytokines such as tumor necrosis factor  $\alpha$  (TNF- $\alpha$ ) and antagonize the activation of the NF- $\kappa$ B pathway by direct and indirect mechanisms.<sup>39</sup> Through this way, DMS has been reported to efficiently decrease the inflammatory toxicity of lipoplexes.<sup>21</sup> For the first time, our study demonstrated that DMS can also decrease the cytotoxicity of nano-carriers based on PEI derivatives.

## Conclusions

In summary, this study demonstrated the possibility of assembling nano-carriers based on a  $\beta$ -CD containing polyelectrolyte and a hydrophobic polymer, a process mediated by host-guest interaction between  $\beta$ -CD and the hydrophobic group. Assemblies formed through this protocol exhibited a core-shell architecture. The hydrophobic core mainly composed of the hydrophobic polymer, can serve as a nano-container to accommodate and sustain the release of hydrophobic drugs. The hydrophilic shell of the positive segment can condense pDNA. Polyplexes thus constructed can achieve the transfection and gene expression of a plasmid DNA. This type of assemblies can simultaneously deliver both small molecular drugs and therapeutic macromolecules including proteins, DNA and siRNA. Furthermore, due to the presence of functionally active amine groups at the periphery, additional functionalities such as stealthy and targeting capability can be conferred to these assemblies by further chemical decoration.

## Experimental Section

### Materials

L-Aspartic acid  $\beta$ -benzyl ester was purchased from Sigma (St. Louis, USA). Triphosgene was obtained from Fisher (USA).  $\beta$ -Benzyl-L-aspartate N-carboxyanhydride (BLA-NCA) was synthesized according to literature.<sup>40</sup> Pyrene ( $\geq 99\%$ ) and  $\beta$ -cyclodextrin ( $\beta$ -CD,  $\geq 98\%$ ) were purchased from Sigma-Aldrich Co. (USA) and used as received. The method established by Baussanne *et al.* was employed to synthesize mono-6-(p-tosyl)- $\beta$ -CD.<sup>41</sup> Dexamethasone (DMS), 1, 6-Diphenyl-1, 3, 5-hexatriene (DPH) and branched polyethyleneimine (PEI) with  $M_w$  of 25, 000 were purchased from Sigma (St. Louis, USA).

### Synthesis of $\beta$ -Cyclodextrin Conjugated Polyethyleneimine (PEI-CD)

1.5 g of branched PEI was dissolved in 15 mL DMSO, into which 10 mL DMSO containing 1.5 g mono-6-(p-tosyl)- $\beta$ -CD was added. The reaction was performed at 75°C for 5 days, and then the polymer was purified by dialysis.

### Synthesis of Poly( $\beta$ -benzyl L-aspartate) (PBLA)

PBLA was synthesized according to a reference.<sup>42</sup> Briefly, 1.5 g BLA-NCA was dissolved in 30 mL anhydrous dioxane at -30°C, into which appropriate amount of n-hexylamine was added to achieve a molar ratio of monomer to initiator of 20:1. Polymerization was performed at room temperature (22°C) for 5 days. After precipitated from diethyl ether, the polymer was dissolved in dichloromethane and precipitated from diethyl ether again. The resultant powder was dried under vacuum. The number-average molecular weight determined by Matrix Assisted Laser Desorption/Ionization Time-of-Flight (MALDI-TOF) mass spectrometer is about 2000.

### Polymer Characterization

<sup>1</sup>H NMR spectra were recorded on a Varian INOVA-400 spectrometer operating at 400 MHz. The MALDI-TOF mass spectrum of PBLA was acquired with a Waters Micromass ToFSpec-2E run in a linear mode. Dithranol (purchased from Aldrich Chemical) was used as a matrix, and tetrahydrofuran as a solvent for both matrix and polymer. The dried-droplet

method was employed in sample preparation.<sup>43</sup> FT-IR spectra were recorded on a Perkin-Elmer FT-IR spectrometer (Spectrum GX).

### Preparation of Assemblies Based on PEI-CD/PBLA

A modified dialysis procedure was used to prepare assemblies or DMS containing assemblies based on PEI-CD and PBLA. In brief, 3.0 mg PBLA dissolved in 1.0 mL DMSO was gradually added into 2.0 mL aqueous solution of PEI-CD (10.0 mg/mL) under sonication. The mixture solution thus obtained was dialyzed against deionized water for 24 h at room temperature. The outer aqueous solution was renewed every 2 hours. For the preparation of DMS-containing assemblies, 3.0 mg PBLA and 3.0 mg DMS were dissolved in 1.0 mL DMSO, which was added dropwise into 2.0 mL deionized water containing 20 mg PEI-CD under bath sonication, and then dialysis was performed. For all the assemblies, characterization was performed after the aqueous solution was filtered through a 0.45  $\mu\text{m}$  syringe filter.

### Fluorescence Measurements

Using pyrene as a fluorophore, steady-state fluorescence spectra were measured on JASCO FP-6200 fluorescence spectrophotometer with a slit width of 5 nm for both excitation and emission. All spectra were run on air-equilibrated solutions. For fluorescence emission spectra, excitation wavelength was set at 339 nm, and for excitation spectra, the emission wavelength was 390 nm. The scanning rate was set at 125 nm/min. All tests were carried out at 25°C. Sample solutions were prepared as described previously.<sup>44</sup> In brief, aqueous copolymer solutions containing pyrene ( $6.0 \times 10^{-7}$  M) were incubated at 50°C for 12 h and subsequently allowed to cool overnight to room temperature.

Fluorescence anisotropy ( $r$ ) was determined with a Fluoromax-2 fluorimeter equipped with an auto-polarizer accessory. The monochromator slits were set at 5.0 nm. 1,6-Diphenyl-1,3,5-hexatriene (DPH) was used as a fluorescence probe. The excitation wavelength was 360 nm, while the emission wavelength was 430 nm. The fluorescence anisotropy was calculated according to the relationship  $r = (I_{VV} - GI_{VH}) / (I_{VV} + 2GI_{VH})$ , where  $G = I_{VH} / I_{HH}$  is an instrumental correction factor and  $I_{VV}$ ,  $I_{VH}$ ,  $I_{HV}$ , and  $I_{HH}$  refer to the emission intensities polarized in the vertical or horizontal detection planes (second subindex) upon excitation with either vertically or horizontally polarized light (first subindex).<sup>45</sup> To prepare sample solutions, a known amount of DPH in methanol was added to 10.0 mL volumetric flasks and the methanol was evaporated. To each flask was then added a stock sample solution, which was heated at 50°C for 12 h and cooled overnight to room temperature. The DPH concentration was kept at  $1.0 \times 10^{-6}$  M. The assemblies' concentration was 5 mg/ml.

### Morphology Study

Transmission electron microscopy (TEM) observation was carried out on a JEOL-3011 high resolution electron microscope operating at an acceleration voltage of 300 kV. Samples were prepared at 25°C by dipping the grid into the aqueous solution of assemblies, and extra solution was blotted with filter paper. After the water was evaporated at room temperature for several days, samples were observed directly without any staining. Formvar coated copper grids, stabilized with evaporated carbon film, were used. Atomic force microscopy (AFM) observation was carried out on a NanoScope IIIa-Phase Atomic force microscope connected to a NanoScope IIIa Controller using an EV scanner. Samples were prepared by drop-casting the dilute solution onto freshly cleaved mica. All the images were acquired under a tapping mode. Scanning electron microscopy (SEM) images were taken on a Field Emission Scanning Electron Microscope (XL30 FEG, Phillips) after a gold layer was coated using a sputter coater (Desk-II, Denton vacuum Inc., Moorstown, NJ) for 100 s. Samples were prepared by coating aqueous solution of assemblies onto freshly cleaved mica, and water was evaporated at room temperature under normal pressure.

### Potentiometric Titration

PEI-CD or PEI-CD/PBLA assemblies were dissolved in 20 mL 0.01 N HCl and titrated with 0.01 N NaOH. The pH values of the solution were determined by a pH meter (Orion 320, Thermo Electron Corporation).

### *In vitro* Release Study

5.0 mg of lyophilized samples of assemblies containing DMS was dissolved into 0.5 mL deionized water, and placed into dialysis tubing, which was immersed into 30 mL PBS (0.1M, pH 7.4). At predetermined time interval, 4.0 mL release medium was withdrawn, and fresh PBS was added. DMS concentration in the release buffer was determined by UV at 265 nm.

### Dynamic Light Scattering (DLS) and $\xi$ -Potential Measurements

DLS and  $\xi$ -potential measurements for the assemblies and assemblies/pDNA based polyplexes in aqueous solutions were performed with a Malvern Zetasizer Nano ZS instrument at 25°C.

### Cells and Plasmid DNA (pDNA)

MC3T3-E1(clone 26) cells were cultured in alpha minimum essential medium ( $\alpha$ -MEM) supplemented with 10% bovine serum, 100 U/mL penicillin and 100  $\mu$ g/mL streptomycin in a humidified incubator at 37°C with 5% CO<sub>2</sub>.<sup>46</sup> The pGL3-Control Vector (Promega, Madison, WI), containing the luciferase gene driven by the SV40 promoter and enhancer, was grown in DH5  $\alpha$  E. coli and purified using Qiagen Hispeed Plasmid Purification kit. The ratio of absorbance at 260 and 280 nm was 1.8 or greater.

### Gel Retardation Analysis

PEI-CD or assemblies sample was dissolved in 10 mM Tris-HCl (pH 7.4) buffer at 1.0 mg/mL, which was then mixed with pDNA in 10 mM Tris-HCl (pH 7.4) (1.0 mg/mL) at varying mass ratios. The mixed solution was diluted to 20  $\mu$ g pDNA/mL by 10 mM Tris-HCl (pH 7.4), followed by an overnight incubation at room temperature. 10  $\mu$ L of each sample (200 ng pDNA) was electrophoresed at 100 V for 0.5 h on a 0.8% agarose gel in 20 mM Tris-acetic acid buffer containing 10 mM sodium acetic acid (pH 7.8). pDNA in the gel was visualized by EtBr(0.5  $\mu$ g/mL) staining.

### Dye Exclusion Assay

Dye exclusion experiment was performed according to literature.<sup>32</sup> Polyplex solutions prepared by mixing pDNA and PEI-CD/PBLA assemblies at different weight ratios, were diluted to 10  $\mu$ g/mL pDNA with ethidium bromide (EtBr, 4.0  $\mu$ g/mL) in 10 mM Tris-HCl (pH 7.4) buffer. The sample solutions were incubated at room temperature overnight. The fluorescence intensity of the samples at 590 nm (excitation at 510 nm) was measured using a spectrofluorometer (Fluoromax-2 fluorimeter). The relative fluorescence intensity was calculated as:  $F_r = (F_s - F_0)/(F_f - F_0)$ , in which  $F_s$ ,  $F_f$ , and  $F_0$  represent the fluorescence intensity of the samples, free pDNA, and background, respectively.

### Polyplexes Formation and Transfection

PEI-CD was dissolved in 20 mM HEPES with 150 mM NaCl (pH 7.3). Polyplexes were prepared by adding 50  $\mu$ L PEI-CD of varying concentrations to an equal volume of 1.0  $\mu$ g pDNA (in Tris-HCl buffer) to achieve the desired polymer/pDNA weight ratio. Polyplexes were then incubated at room temperature for 20 min. Cells were plated in 24-well plates at high density 24 h prior to transfection. Immediately before transfection, the growth medium was replaced with serum-free medium (500  $\mu$ L/well), and 50  $\mu$ L polyplexes solution (1.0  $\mu$ g plasmid/well) was added to each well. Transfection medium was replaced with fresh growth



medium 5 h post-transfection. Luciferase expression was quantified 48 h later using a Promega luciferase assay system. Luciferase activity was measured in relative light units (RLU) using luminometer. Results were normalized to total cell protein as determined using a Pierce Micro BCA Protein Assay. All samples were run in triplicate and on three or more separate occasions. By the similar protocol, polyplexes based on PEI-CD/PBLA assemblies and DMS containing assemblies were evaluated.

### Cytotoxicity Determination

The cytotoxicity of polyplexes was tested using a Promega CellTiter 96 AQueous One Solution Cell Proliferation Assay. Briefly, cells were plated in 24-well plates at  $1 \times 10^5$  cells/well and cultured for 24 h. Polyplexes were then added to each well. After 24 h of incubation, the medium was changed to fresh medium (400  $\mu$ L/well) and 40  $\mu$ L of MTS solution was added to each well. The plates were then incubated in a 5% CO<sub>2</sub> incubator at 37°C for 1 h. The absorbance of the medium from each well was read at 490 nm with an ELISA plate reader. The experiment was performed in triplicate.

### Supplementary Material

Refer to Web version on PubMed Central for supplementary material.

### Acknowledgments

The authors would like to acknowledge the financial support from the NIH (NIDCR DE015384 & DE017689). The authors gratefully acknowledge Prof. K Kuroda for making the fluorescence spectrophotometer available and Prof. NA Kotov for making DLS instrument available for this project.

### References and Notes

1. Torchilin VP. Multifunctional Nanocarriers. *Adv Drug Deliv Rev* 2006;58:1532–1555. [PubMed: 17092599]
2. Kim J, Park S, Lee JE, Jin SM, Lee JH, Lee IS, Yang I, Kim JS, Kim SK, Cho MH, Hyeon T. Designed Fabrication of Multifunctional Magnetic Gold Nanoshells and Their Application to Magnetic Resonance Imaging and Photothermal Therapy. *Angew Chem Int Ed* 2006;45:7754–7758.
3. Kim JS, Rieter WJ, Taylor KML, An HY, Lin WL, Lin WB. Self-Assembled Hybrid Nanoparticles for Cancer-Specific Multimodal Imaging. *J Am Chem Soc* 2007;129:8962–8963. [PubMed: 17602632]
4. Huang CK, Lo CL, Chen HH, Hsiue GH. Multifunctional Micelles for Cancer Cell Targeting, Distribution Imaging, and Anticancer Drug Delivery. *Adv Funct Mater* 2007;17:2291–2297.
5. Li YY, Cheng H, Zhang ZG, Wang C, Zhu JL, Liang Y, Zhang KL, Cheng SX, Zhang XZ, Zhuo RX. Cellular Internalization and in Vivo Tracking of Thermosensitive Luminescent Micelles Based on Luminescent Lanthanide Chelate. *ACS Nano* 2008;2:125–133. [PubMed: 19206556]
6. Liong M, Lu J, Kovochich M, Xia T, Ruehm SG, Nel AE, Tamanoi F, Zink JI. Multifunctional Inorganic Nanoparticles for Imaging, Targeting, and Drug Delivery. *ACS Nano* 2008;2:889–896. [PubMed: 19206485]
7. Kim J, Lee JE, Lee SH, Yu JH, Lee JH, Park TG, Hyeon T. Designed Fabrication of a Multifunctional Polymer Nanomedical Platform for Simultaneous Cancer-Targeted Imaging and Magnetically Guided Drug Delivery. *Adv Mater* 2008;20:478–483.
8. Rieter WJ, Kim JS, Taylor KML, An HY, Lin WL, Tarrant T, Lin WB. Hybrid Silica Nanoparticles for Multimodal Imaging. *Angew Chem Int Ed* 2007;46:3680–3682.
9. Kim S, Ohulchanskyy TY, Pudavar HE, Pandey RK, Prasad PN. Organically Modified Silica Nanoparticles Co-encapsulating Photosensitizing Drug and Aggregation-Enhanced Two-Photon Absorbing Fluorescent Dye Aggregates for Two-Photon Photodynamic Therapy. *J Am Chem Soc* 2007;129:2669–2675. [PubMed: 17288423]

10. Qi LF, Gao XH. Quantum Dot-Amphipol Nanocomplex for Intracellular Delivery and Real-Time Imaging of siRNA. *ACS Nano* 2008;2:1403–1410. [PubMed: 19206308]
11. Nehilla BJ, Allen PG, Desai TA. Surfactant-Free, Drug-Quantum-Dot Coloaded Poly(lactide-co-glycolide) Nanoparticles: Towards Multifunctional Nanoparticles. *ACS Nano* 2008;2:538–544. [PubMed: 19206580]
12. Ghosh PS, Kim CK, Han G, Forbes NS, Rotello VM. Efficient Gene Delivery Vectors by Tuning the Surface Charge Density of Amino Acid-Functionalized Gold Nanoparticles. *ACS Nano* 2008;1:2213–2218. [PubMed: 19206385]
13. Al-Jamal WT, Al-Jamal KT, Tian B, Lacerda L, Bomans PH, Frederik PM, Kostarelos K. Lipid-Quantum Dot Bilayer Vesicles Enhance Tumor Cell Uptake and Retention in Vitro and in Vivo. *ACS Nano* 2008;2:408–418. [PubMed: 19206564]
14. Farokhzad OC, Langer R. Impact of Nanotechnology on Drug Delivery. *ACS Nano* 2009;3:16–20. [PubMed: 19206243]
15. Medarova Z, Pham W, Farrar C, Petkova V, Moore A. In vivo Imaging of siRNA Delivery and Silencing in Tumors. *Nat Med* 2007;13:372–377. [PubMed: 17322898]
16. Yezhelyev MV, Qi LF, O'Regan RM, Nie SM, Gao XH. Proton-Sponge Coated Quantum Dots for siRNA Delivery and Intracellular Imaging. *J Am Chem Soc* 2008;130:9006–9012. [PubMed: 18570415]
17. Malone RW, Hickman MA, Lehmann-Bruinsma K, Sih TR, Walzem R, Carlson DM, Powell JS. Dexamethasone Enhancement of Gene Expression after Direct Hepatic DNA Injection. *J Biol Chem* 1994;269:29903–29907. [PubMed: 7961986]
18. Zhang XH, Collins L, Sawyer GJ, Dong XB, Qiu Y, Fabre JW. In Vivo Gene Delivery via Portal Vein and Bile Duct to Individual Lobes of the Rat Liver Using a Polylysine-Based Nonviral DNA Vector in Combination with Chloroquine. *Hum Gene Ther* 2001;12:2179–2190. [PubMed: 11779402]
19. Kishida T, Asada H, Itokawa Y, Yasutomi K, Shin-Ya M, Gojo S, Cui FD, Ueda Y, Yamagishi H, Imanishi J, Mazda O. Electrochemo-Gene Therapy of Cancer: Intratumoral Delivery of Interleukin-12 Gene and Bleomycin Synergistically Induced Therapeutic Immunity and Suppressed Subcutaneous and Metastatic Melanomas in Mice. *Mol Ther* 2003;8:738–745. [PubMed: 14599806]
20. Janat-Amsbury MM, Yockman JW, Lee M, Kern S, Furgeson DY, Bikram M, Kim SW. Combination of Local, Nonviral IL12 Gene Therapy and Systemic Paclitaxel Treatment in a Metastatic Breast Cancer Model. *Mol Ther* 2004;9:829–836. [PubMed: 15194049]
21. Liu F, Shollenberger LM, Huang L. Non-immunostimulatory Nonviral Vectors. *FASEB J* 2004;18:1779–1781. [PubMed: 15364893]
22. Wang Y, Gao SJ, Ye WH, Yoon HS, Yang YY. Co-delivery of Drugs and DNA from Cationic Core-shell Nanoparticles Self-assembled from a Biodegradable Copolymer. *Nat Mater* 2006;5:791–796. [PubMed: 16998471]
23. Qiu LY, Bae YH. Self-assembled Polyethylenimine-graft-poly( $\epsilon$ -caprolactone) Micelles as Potential Dual Carriers of Genes and Anticancer Drugs. *Biomaterials* 2007;28:4132–4142. [PubMed: 17582489]
24. Davis ME, Brewster ME. Cyclodextrin-Based Pharmaceuticals: Past, Present and Future. *Nat Rev Drug Discov* 2004;3:1023–1035. [PubMed: 15573101]
25. Cheng JJ, Khin KT, Jensen GS, Liu AJ, Davis ME. Synthesis of Linear,  $\beta$ -Cyclodextrin-Based Polymers and Their Camptothecin Conjugates. *Bioconjugate Chem* 2003;12:1007–1017.
26. Numbenjapon T, Wang JY, Colcher D, Schlupe T, Davis ME, Durringer J, Kretzner L, Yen Y, Forman SJ, Raubitschek A. Preclinical Results of Camptothecin-Polymer Conjugate (IT-101) in Multiple Human Lymphoma Xenograft Models. *Clin Cancer Res* 2009;15:4365–4373. [PubMed: 19549776]
27. Bartlett DW, Davis ME. Physicochemical and Biological Characterization of Targeted, Nucleic Acid-Containing Nanoparticles. *Bioconjugate Chem* 2007;18:456–468.
28. Heidel JD, Yu ZP, Liu JY, Rele SM, Liang YC, Zeidan RK, Kornbrust DJ, Davis ME. Administration in Non-Human Primates of Escalating Intravenous Doses of Targeted Nanoparticles Containing Ribonucleotide Reductase Subunit M2 siRNA. *Proc Natl Acad Sci USA* 2007;104:5715–5721. [PubMed: 17379663]

29. Rekharsky MV, Inoue Y. Complexation Thermodynamics of Cyclodextrins. *Chem Rev* 1998;98:1875–1917. [PubMed: 11848952]
30. Miyata K, Kakizawa Y, Nishiyama N, Yamasaki Y, Watanabe T, Kohara M, Kataoka K. Freeze-Dried Formulations for in vivo Gene Delivery of PEGylated Polyplex Micelles with Disulfide Crosslinked Cores to the Liver. *J Control Release* 2005;109:15–23. [PubMed: 16298011]
31. Lepecq JB, Paoletti C. A Fluorescent Complex between Ethidium Bromide and Nucleic Acids Physical—Chemical Characterization. *J Mol Biol* 1967;27:87–106. [PubMed: 6033613]
32. Kanayama N, Fukushima S, Nishiyama N, Itaka K, Jang WD, Miyata K, Yamasaki Y, Chung U, Kataoka K. A PEG-Based Biocompatible Block Cationic Polymer with High Buffering Capacity for the Construction of Polyplex Micelles Showing Efficient Gene Transfer toward Primary Cells. *ChemMedChem* 2006;1:439–444. [PubMed: 16892379]
33. Wakebayashi D, Nishiyama N, Itaka K, Miyata K, Yamasaki Y, Harada A, Koyama H, Nagasaki Y, Kataoka K. Polyion Complex Micelles of pDNA with Acetal-poly(ethylene glycol)-poly(2-(dimethylamino)ethyl methacrylate) Block Copolymer as the Gene Carrier System: Physicochemical Properties of Micelles Relevant to Gene Transfection Efficacy. *Biomacromolecules* 2004;5:2128–2136. [PubMed: 15530026]
34. Itaka K, Yamauchi K, Harada A, Nakamura K, Kawaguchi H, Kataoka K. Polyion Complex Micelles from Plasmid DNA and Poly(ethylene glycol)-Poly(L-lysine) Block Copolymer as Serum-Tolerable Polyplex System: Physicochemical Properties of Micelles Relevant to Gene Transfection Efficiency. *Biomaterials* 2003;24:4495–4506. [PubMed: 12922159]
35. Harada A, Kataoka K. Novel Polyion Complex Micelles Entrapping Enzyme Molecules in the Core. 2. Characterization of the Micelles Prepared at Nonstoichiometric Mixing Ratios. *Langmuir* 1999;15:4208–4212.
36. Kastrop L, Oberleithner H, Ludwig Y, Schafer C, Shahin V. Nuclear Envelope Barrier Leak Induced by Dexamethasone. *J Cell Physiol* 2006;206:428–434. [PubMed: 16110478]
37. Rebuffat A, Bernasconi A, Ceppi M, Wehrli H, Verca SB, Ibrahim M, Frey BM, Frey FJ, Rusconi S. Selective Enhancement of Gene Transfer by Steroid-Mediated Gene Delivery. *Nat Biotechnol* 2001;19:1155–1161. [PubMed: 11731785]
38. Dames P, Laner A, Maucksch C, Aneja MK, Rudolph C. Targeting of the Glucocorticoid Hormone Receptor with Plasmid DNA Comprising Glucocorticoid Response Elements Improves Nonviral Gene Transfer Efficiency in the Lungs of Mice. *J Gene Med* 2007;9:820–829. [PubMed: 17668918]
39. Zingarelli B, Sheehan M, Wong HR. Nuclear Factor- $\kappa$ B as a Therapeutic Target in Critical Care Medicine. *Crit Care Med* 2003;31:S105–S111. [PubMed: 12544984]
40. Daly WH, Poché D. The Preparation of N-Carboxyanhydrides of Alpha-Amino-Acids Using Bis (trichloromethyl) Carbonate. *Tetrahedron Lett* 1988;29:5859–5862.
41. Baussanne I, Benito JM, Mellet CO, Fernández JMG, Law H, Defaye J. Synthesis and Comparative Lectin-Binding Affinity of Mannosyl-Coated Beta-Cyclodextrin-Dendrimer Constructs. *Chem Commun* 2000:1489–1490.
42. Blout ER, Karlson RH. Polypeptides. 3. The Synthesis of High Molecular Weight Poly-Gamma-L-Glutamates. *J Am Chem Soc* 1956:941–946.
43. Montaudo G, Montaudo MS, Puglisi C, Samperi F. Characterization of Polymers by Matrix-Assisted Laser-Desorption Ionization-Time of Flight Mass Spectrometry-End Group Determination and Molecular-Weight Estimates in Poly(ethylene glycols). *Macromolecules* 1995;28:4562–4569.
44. Wilhelm M, Zhao CL, Wang YC, Xu RL, Winnik MA, Mura JL, Riess G, Croucher MD. Polymer Micelle Formation. 3. Poly(styrene-ethylene oxide) Block Copolymer Micelle Formation in Water-A Fluorescence Probe Study. *Macromolecules* 1991;24:1033–1040.
45. Ringsdorf H, Venzmer J, Winnik FM. Fluorescence Studies of Hydrophobically Modified Poly(N-isopropylacrylamides). *Macromolecules* 1991;24:1678–1686.
46. Chen VJ, Smith LA, Ma PX. Bone Regeneration on Computer-Designed Nano-fibrous Scaffolds. *Biomaterials* 2006;27:3973–3979. [PubMed: 16564086]

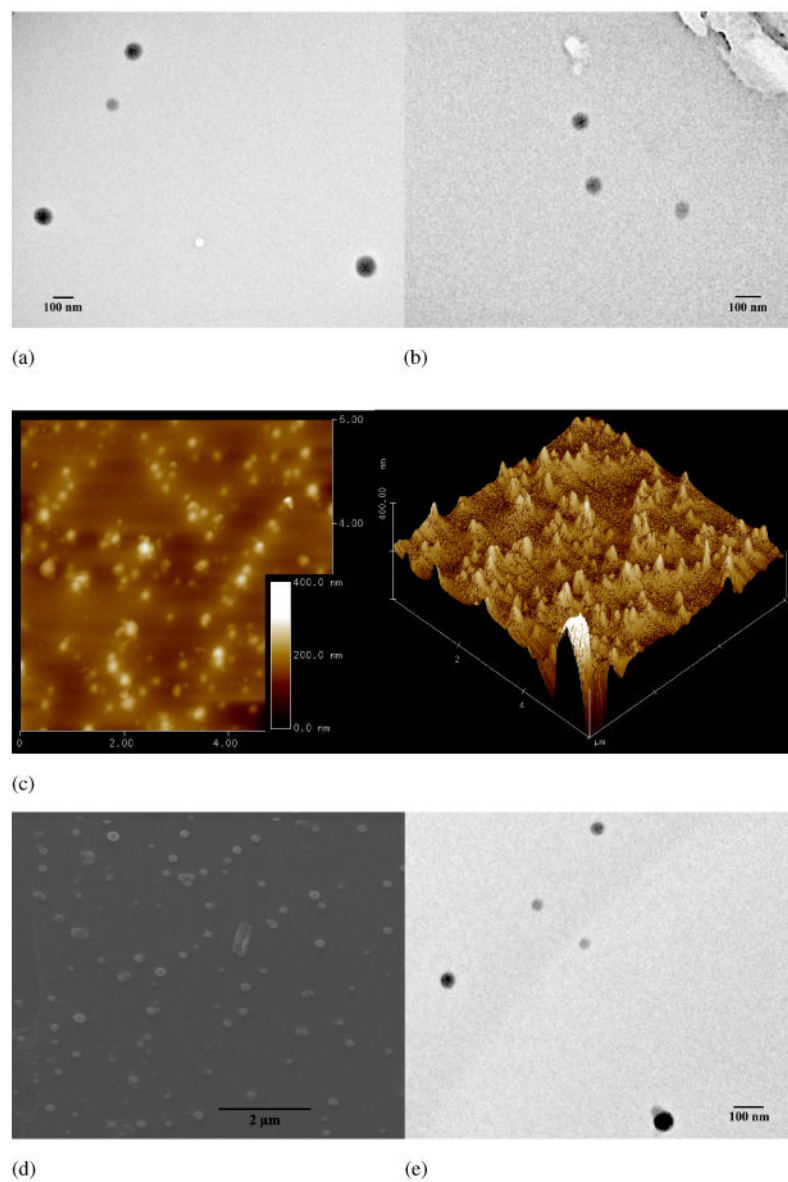


**Figure 1.** TEM images of assemblies based on PEI-CD/PBLA before (a) and after freeze-drying reconstitution (b); (c) AFM images of assemblies; (d) SEM image; and (e) TEM image of assemblies containing dexamethasone (DMS).

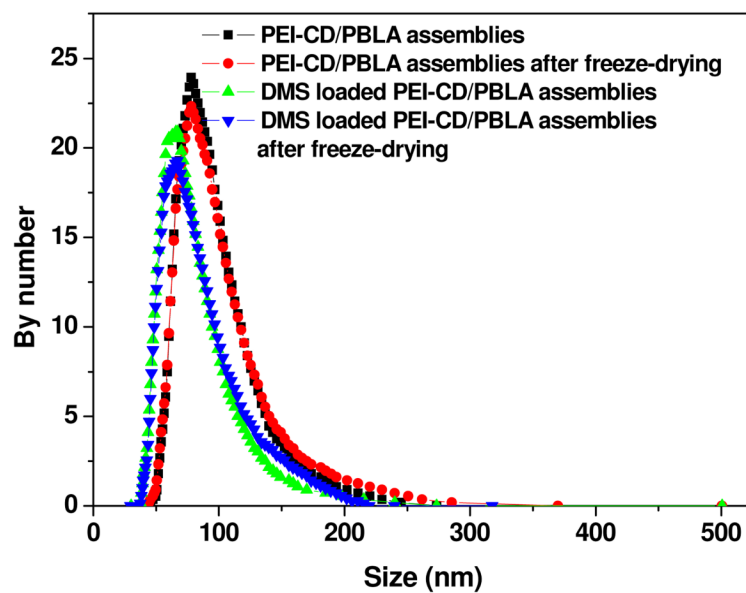


**Figure 2.**  
Size distribution of assemblies based on PEI-CD/PBLA with or without DMS.

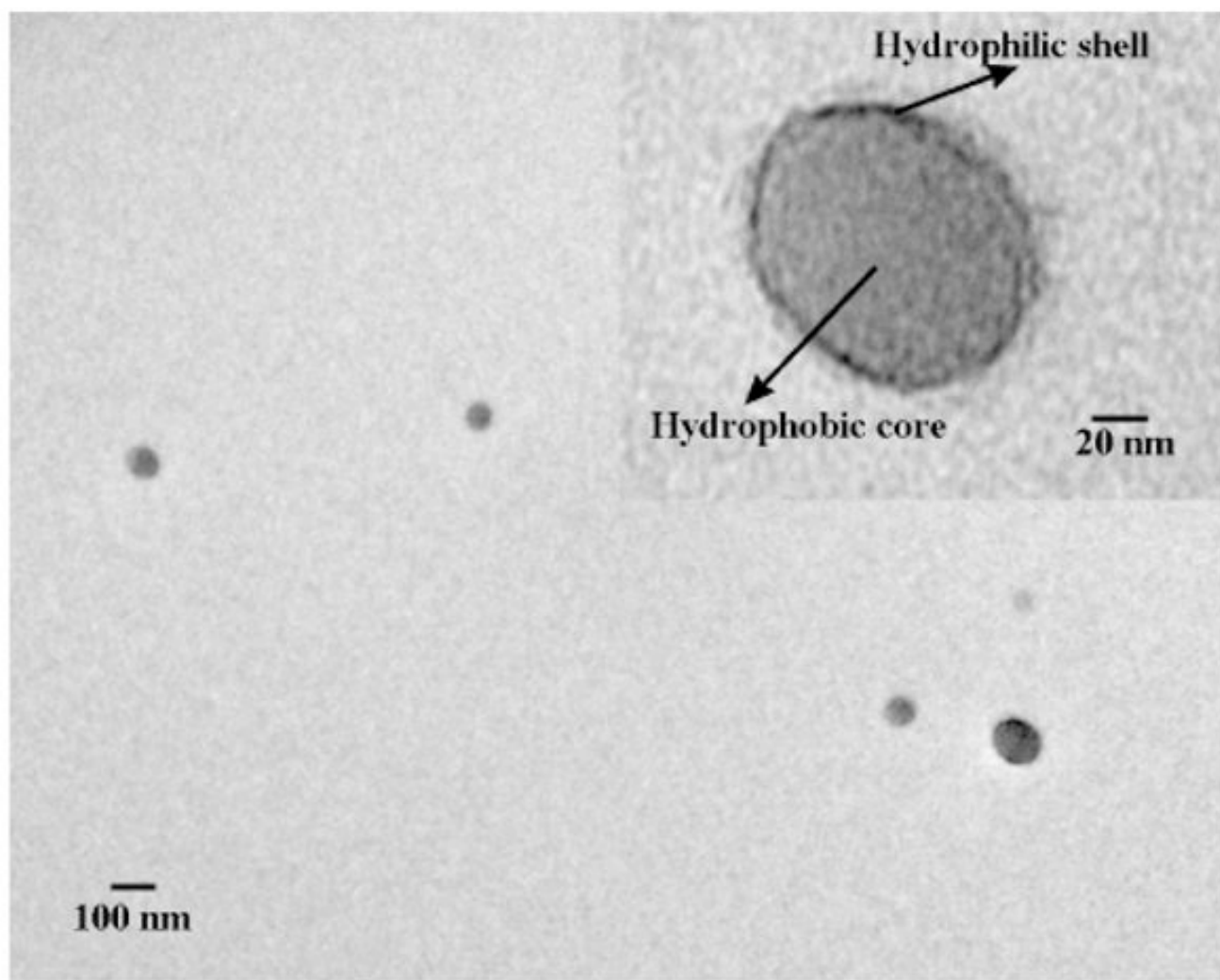


**Figure 3.**  
TEM image of PEI-CD/PBLA assemblies after staining with phosphotungstic acid.

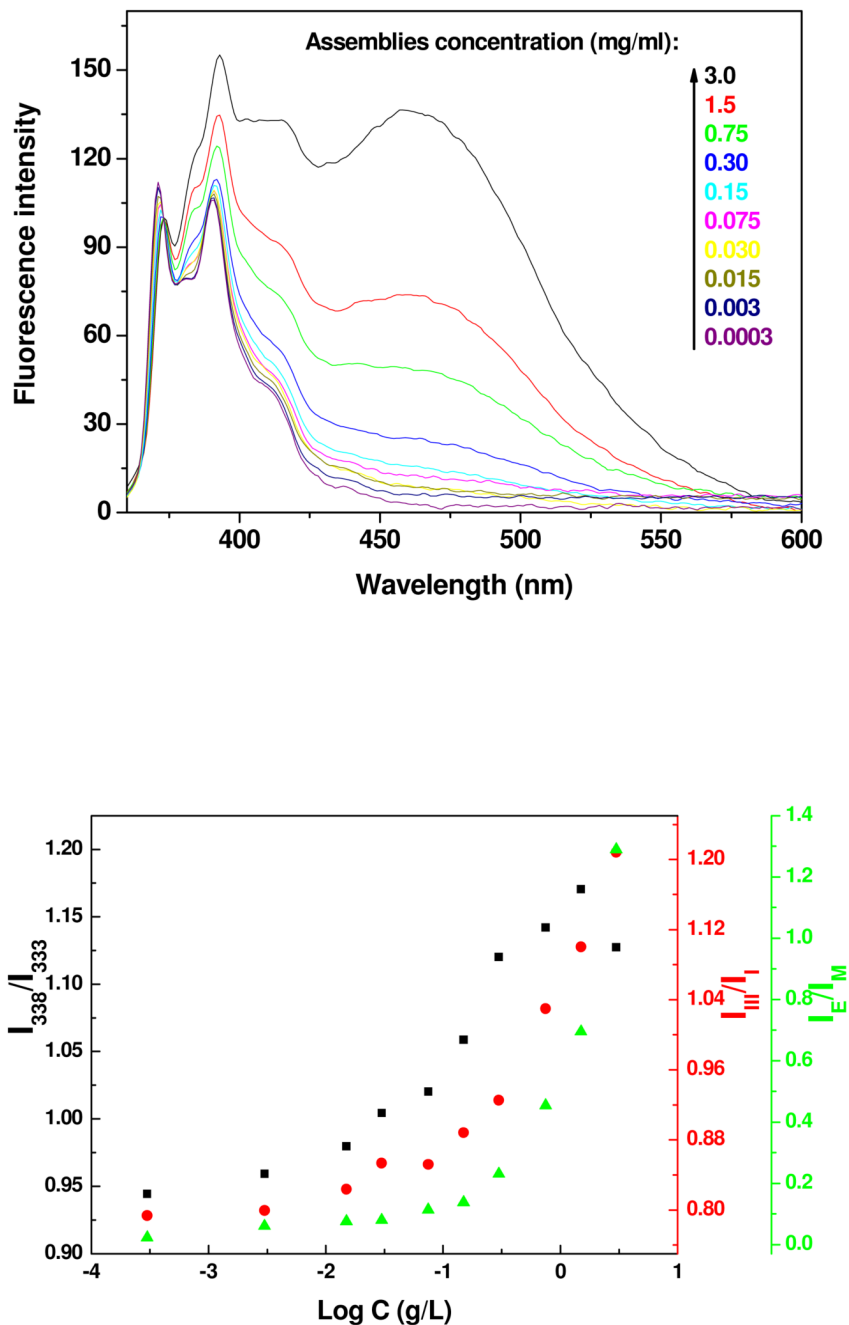


**Figure 4.** (a) Normalized emission spectra of pyrene in aqueous solutions containing various concentrations of PEI-CD/PBLA; (b) Plots of  $I_{338}/I_{333}$ ,  $I_3/I_1$  and  $I_E/I_M$  as a function of PEI-CD/PBLA concentration.  $I_{338}/I_{333}$  -- the ratio of intensity at 338 nm to that at 333 nm in the (0, 0) band of pyrene excitation spectrum;  $I_3/I_1$  -- the intensity ratio between the third and first vibrational bands in pyrene emission spectrum;  $I_E/I_M$  -- the intensity ratio of the excimer (475 nm) to monomer (371 nm) in emission spectrum.  $[\text{Pyrene}] = 6.0 \times 10^{-7} \text{ M}$ .

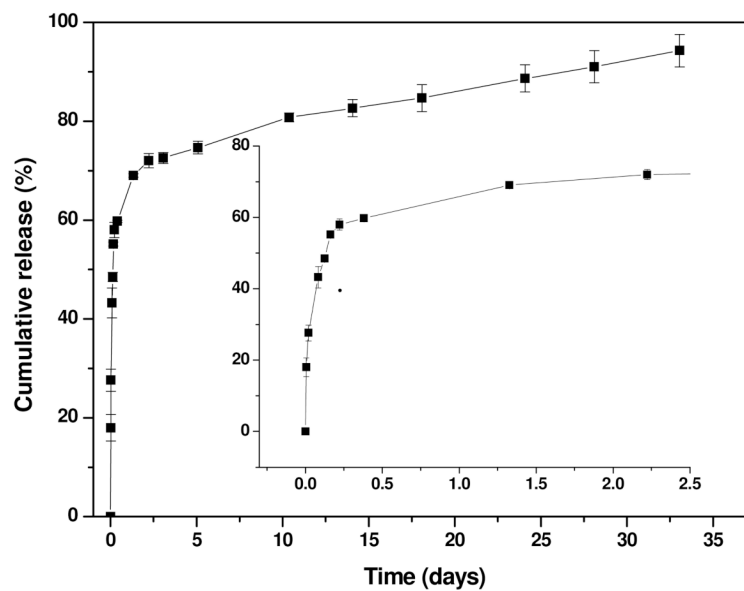


**Figure 5.**  
*In vitro* DMS release profile from DMS-containing PEI-CD/PBLA assemblies.



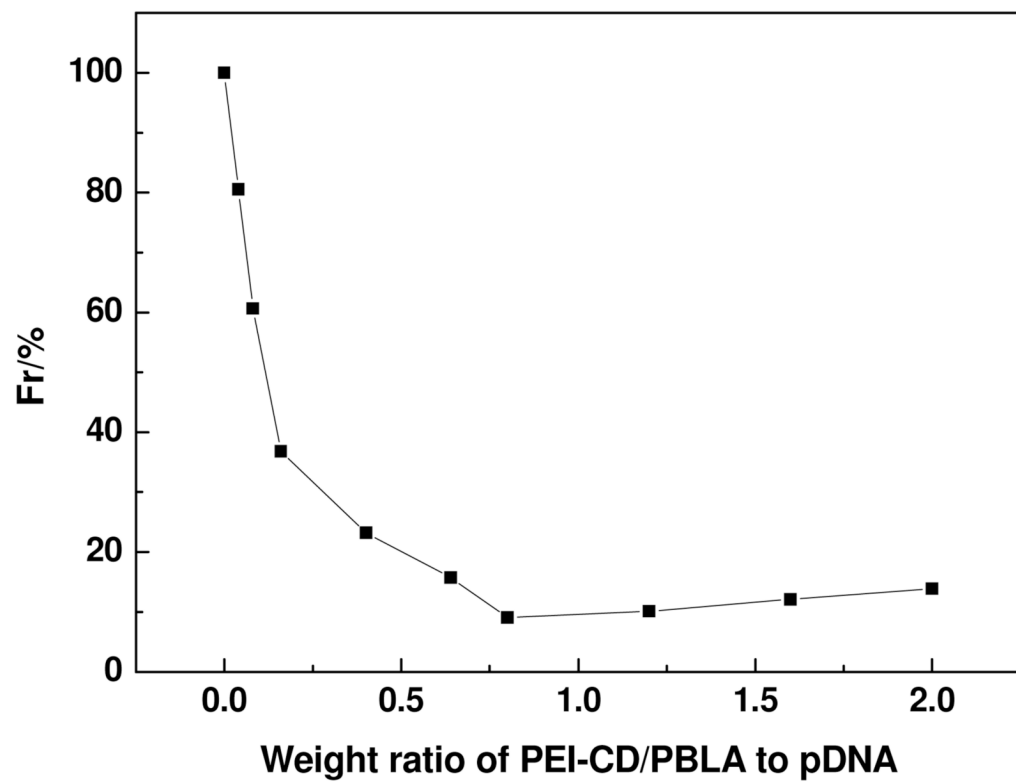
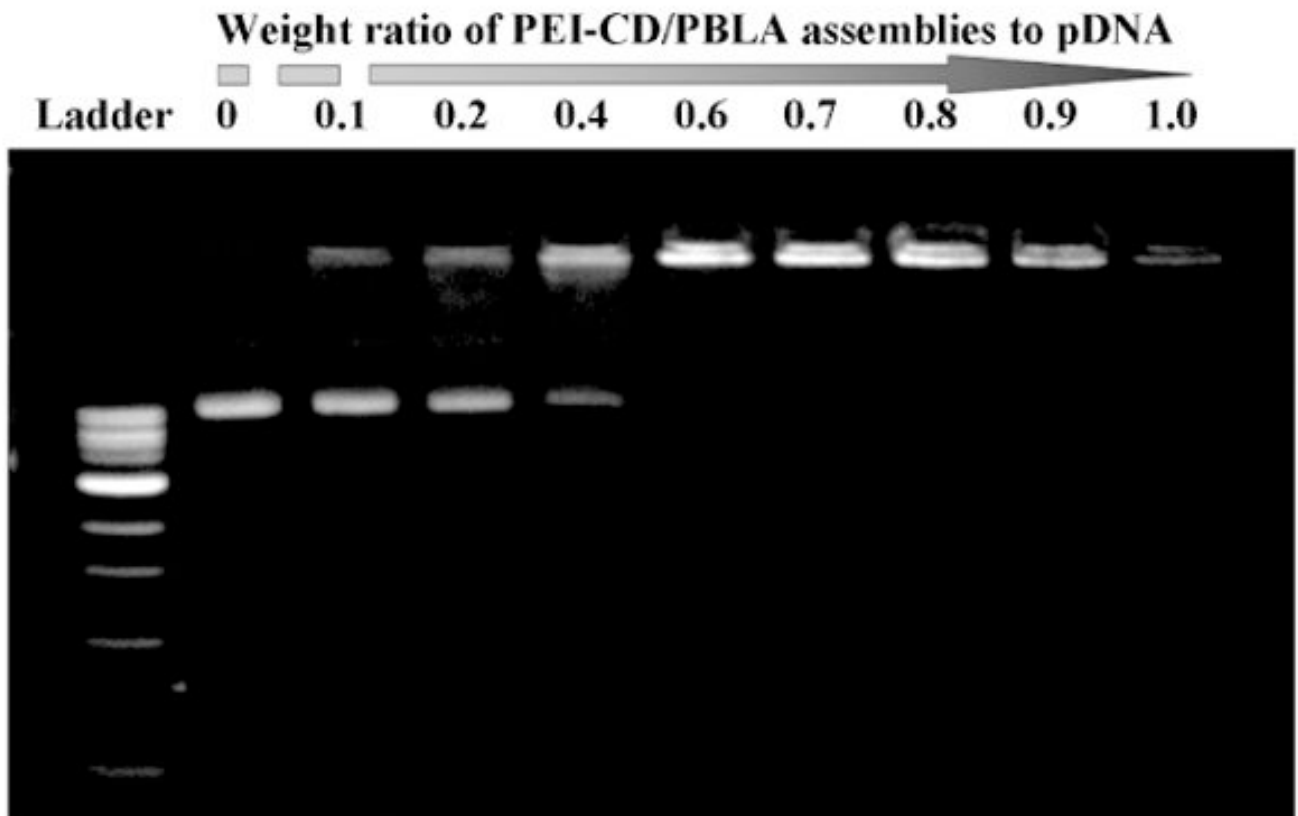


**Figure 6.**

(a) Gel retardation assay of PEI-CD/PBLA assemblies and pDNA; (b) Relative fluorescence intensity (Fr) of EtBr in solution with pDNA and PEI-CD/PBLA assemblies at various weight ratios.

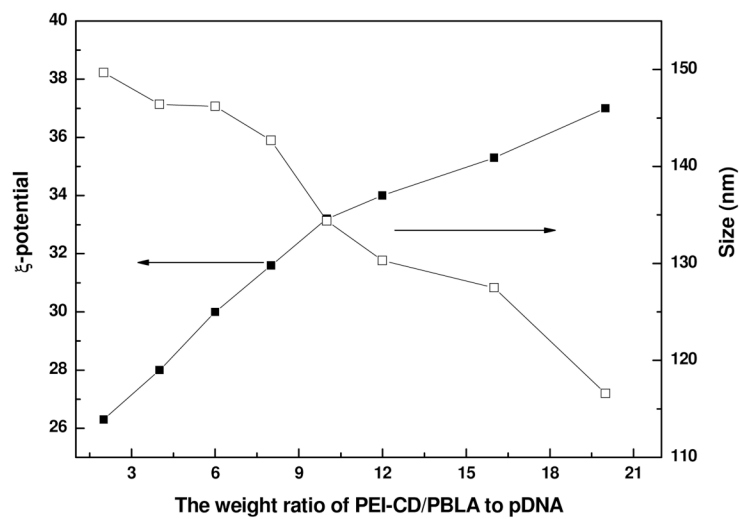
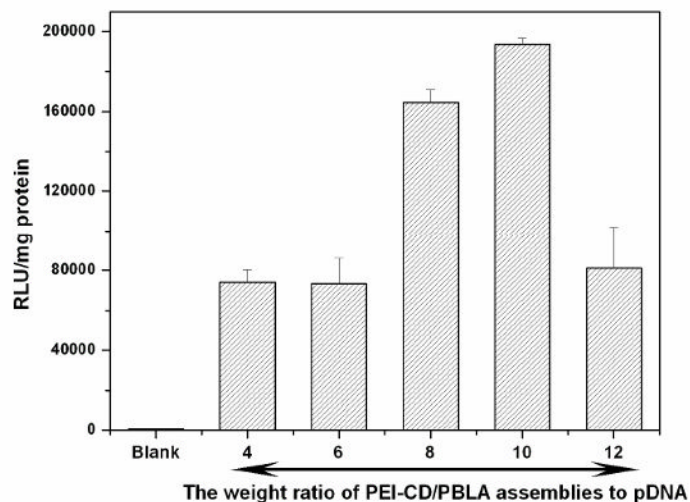
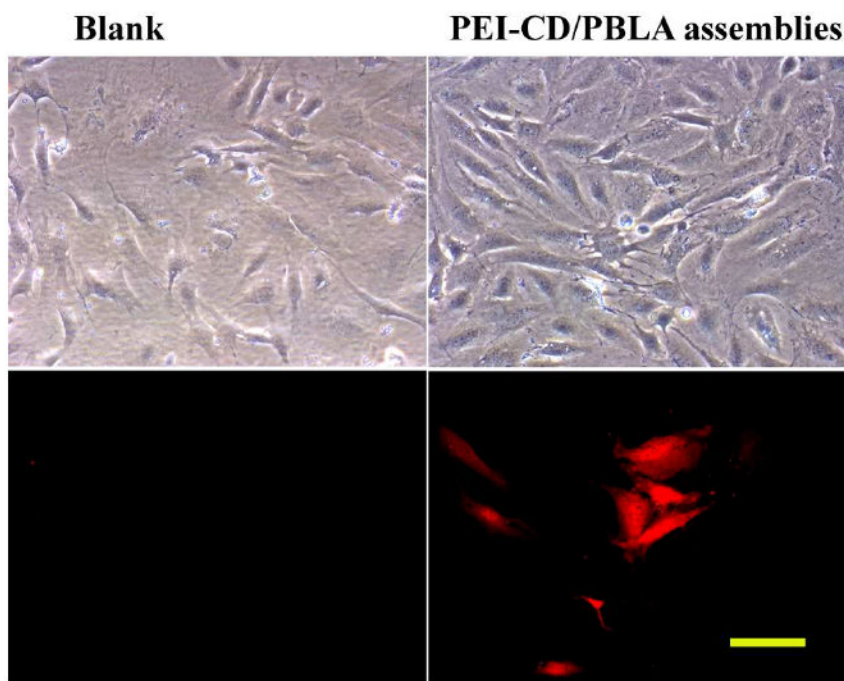


**Figure 7.**  $\zeta$ -Potential and particle size of polyplexes based on PEI-CD/PBLA assemblies and pDNA with various weight ratios.



(a)



(b)

**Figure 8.**

(a) *In vitro* transfection of the luciferase gene into osteoblast cells by PEI-CD/PBLA nano-assemblies. Luciferase activity (RLU) was quantified using luminometer 48 h after cells were transfected. Results were normalized to total cell protein. All samples were run in triplicate and on three or more separate occasions. (b) The transfected cells were viewed by a fluorescence microscope (Nikon Eclipse 50i microscope) 48 h after transfection. Excitation was performed with green light. Polyplexes with the weight ratio of PEI-CD/PBLA to pDNA of 8 were employed. The scale bar represents 100  $\mu\text{m}$ .

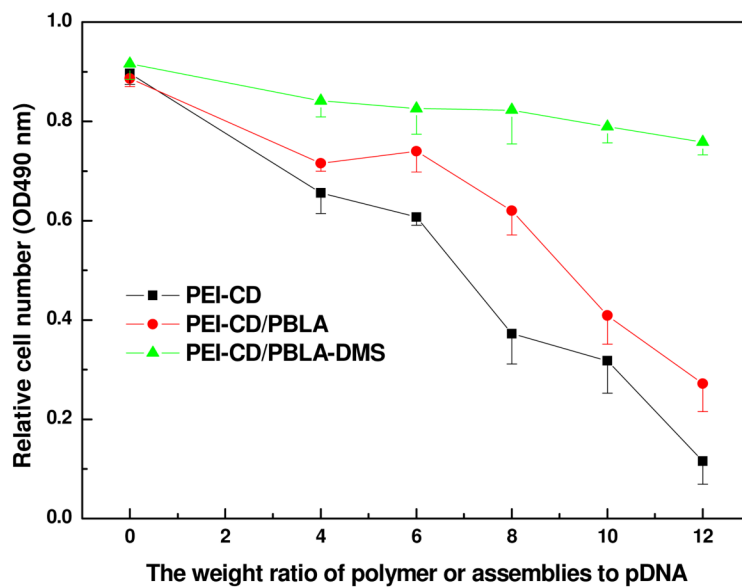


**Figure 9.** Cytotoxicity of PEI-CD/PBLA assemblies and DMS containing assemblies against osteoblast cells. After incubation for 24 h with the solutions of different polyplexes, the cell viability was detected using a Promega CellTiter 96 AQueous One Solution Cell Proliferation Assay. The experiment was performed in triplicate.

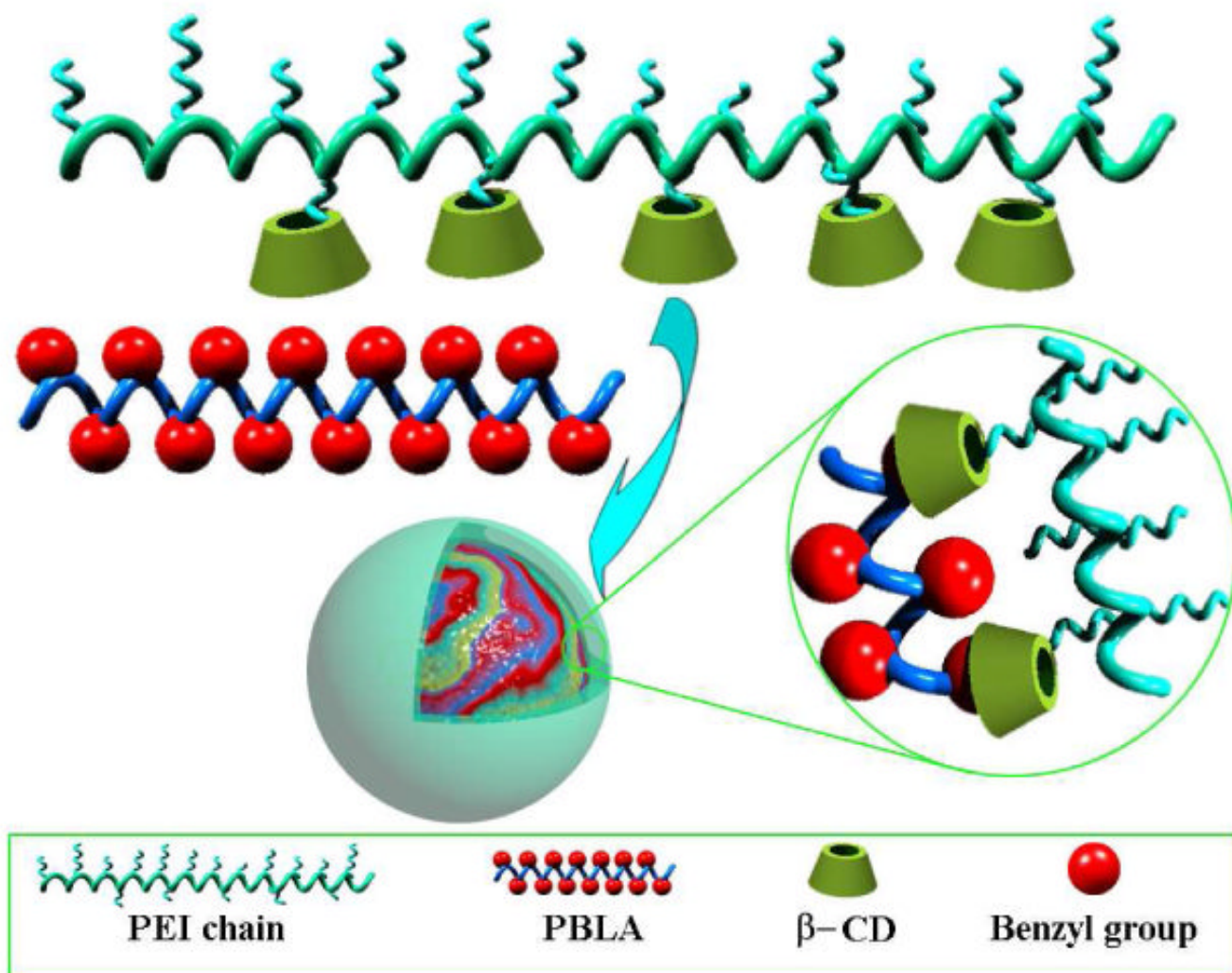
**Scheme 1.**

Illustration of the core-shell nano-assemblies based on PEI-CD/PBLA by host-guest interaction.